THE ASTROPHYSICAL JOURNAL, 560:719–729, 2001 October 20

COSMIC-RAY PRODUCTION AND THE ROLE OF SUPERNOVAE IN NGC 6946

C. K. LACEY[1]
Naval Research Laboratory, Code 7213, 4555 Overlook Avenue, SW, Washington, DC 20375; lacey@rsd.nrl.navy.mil
AND
N. DURIC
University of New Mexico, Institute for Astrophysics, Department of Physics and Astronomy,
University of New Mexico, 800 Yale NE, Albuquerque, NM 87131
Received 2000 July 26; accepted 2001 June 25

ABSTRACT

We present a study of 35 radio-selected supernova remnant (SNR) candidates in the nearby spiral galaxy NGC 6946. In this study, an optically selected sample of 27 SNRs from Matonick & Fesen is compared to our sample of radio-selected SNRs. The optically selected SNRs are found to have almost no overlap with the radio-selected sample. This dichotomy is further enhanced by the observation that the optically selected SNRs favor the interarm regions, while the radio-emitting SNRs lie predominately on the spiral arms in or near regions of high star formation. The separation of the two samples of SNRs is discussed in terms of selection effects and differences in cosmic-ray production. The optical sample of SNRs is probably biased toward those SNRs located in areas of NGC 6946 where the confusion of Hα emission by H II regions is relatively low and the SNRs are easier to identify by their emission-line signatures. The radio-selected sample is also subject to selection biases such that these SNRs favor the arms. However, the absence of radio emission from the optically selected, largely interarm SNRs and the relatively large number of radio-detected SNRs in the arms require additional explanation. The properties of the radio-selected SNRs are discussed in the context of diffusive shock acceleration theory. We find that the theory can account for the range in radio flux densities and the nondetection of the optically selected SNRs. The differences in the radio properties between the arm and interarm population of SNRs can be explained by differences in the average gas densities and magnetic fields since the latter affect both the cosmic-ray yield and the radio properties of the SNRs. The possibility that the arm and interarm SNRs arise from different stellar populations is also addressed.

Subject headings: acceleration of particles — cosmic rays — galaxies: individual (NGC 6946) — galaxies: ISM — supernova remnants

1. INTRODUCTION

Supernova remnants (SNRs) have become the favored candidates for the acceleration of cosmic rays (CRs). There exists a widely accepted acceleration mechanism, diffusive shock acceleration (DSA), in which the expanding shock of the SNR accelerates the CRs. While there are many unresolved issues in DSA theory, such as how the CRs are injected, the amplification of magnetic fields, and details of the exact shock/CR interaction, DSA has been generally successful in describing observed radio emission from SNRs. Recently, DSA models have been applied to SN 1987A (Duffy, Lewis, & Kirk 1995) and Cassiopeia A (Anderson & Rudnick 1996). In both cases, DSA was shown to be necessary to explain the observed radio emission. However, these SNRs are young, and there remains the important question of how the DSA mechanism operates in a population of SNRs, that is, in SNRs of various ages, in a wide range of environments, and in SNRs arising from different stellar precursors.

The link between CRs and the SNR precursor cannot be probed from the study of individual SNRs since most SNRs are thousands of years old and no direct information exists on the progenitor stars. While the sample of Galactic SNRs is the largest sample available, it is not an ideal sample to study because of severe observational biases including high levels of radio continuum confusion, especially toward the Galactic center, and poorly determined distances to individual SNRs. These factors, plus the poor perspective from inside the Milky Way, all preclude straightforward identification of Galactic SNRs with a progenitor stellar population.

For these reasons, studies of SNRs are increasingly turning to external galaxies, in which the more favorable orientation and perspective provide not only equidistant samples of SNRs but also minimize both extinction and confusion. High-resolution studies of nearby galaxies (angular resolution $\sim 1''$) have recently been undertaken to address the morphology of discrete radio sources and correlate the results with other wavelengths. Gordon et al. (1999) found 53 radio-selected SNRs in M33 but were not able to identify the SNRs with a specific population of progenitors.

If SNRs could be associated with the spiral arms, then massive stars would be indicated as the progenitors of the SNRs. A preliminary study of NGC 6946 (Lacey & Duric 1997) yielded a result linking the radio-selected SNRs to the spiral arms and massive stellar progenitors. In this paper, we present a study of 35 radio-selected SNR candidates in the nearby spiral galaxy NGC 6946, identified from obser-

[1] Naval Research Lab/National Research Council Cooperative Research Associate. Current address: Department of Physics and Astronomy, University of South Carolina, Columbia, SC 29208; lacey@sc.edu.

TABLE 1

OBSERVING PARAMETERS FOR NGC 6946

Date Observed (1994)	Wavelength (cm)	RMS Sensitivity (μJy beam^{-1})	Field of View (arcmin)	Angular Resolution (arcsec)
Apr 1.....	20	20	30	1.5
Jun 16–17.....	6	16	9	1.5

vations taken with the NRAO VLA[2] (Lacey, Duric, & Goss 1997).

The main goal of this paper is to describe an analysis of the SNRs in NGC 6946 and make the case that environment and possibly initial conditions play an important role in shaping the spectral properties of SNRs. We specifically address the issue of CR yield and its relation to the environment of an SNR as well as the selection effects that make multiwavelength studies of SNRs critical to the characterization of the SNR population.

[2] The National Radio Astronomy Observatory is a facility of the National Science Foundation operated under cooperative agreement by Associated Universities, Inc.

2. THE SAMPLE OF SNRS IN NGC 6946

NGC 6946, a nearby spiral galaxy with coordinates (B1950) R.A. = $20^{h}33^{m}49^{s}.245$, decl. = $+59°58'49''.24$ (Van Dyk et al. 1994), is a good candidate to search for compact extragalactic radio sources. NGC 6946 is a roughly face-on spiral galaxy of Hubble-type Scd manifesting six historical SNe in the past 100 yr. The small inclination angle ($i \sim 30°$; Rogstad & Shostak 1973) of NGC 6946 results in minimal internal radio confusion and aids in the identification of radio sources with optical counterparts. The galaxy is undergoing a starburst phase in the nucleus (Ball et al. 1985), which combined with the history of recent supernovae, indicates that NGC 6946 has a rich, young stellar population. The distance to NGC 6946 is not well known,

TABLE 2

CATALOG OF CANDIDATE RADIO SNRS

ID Number (1)	R.A. (B1950) (2)	Decl. (B1950) (3)	S_{20} (mJy) (4)	δS_{20} (mJy) (5)	S_6 (mJy) (6)	δS_6 (mJy) (7)	α (8)	$\delta\alpha$ (9)
8	20 33 28.0	59 58 03.8	0.200	0.030	0.100	0.030	0.500	0.300
12.....	20 33 31.9	60 01 09.7	0.180	0.040	0.090	0.030	0.600	0.300
13.....	20 33 32.0	60 01 14.6	0.630	0.070	0.400	0.060	0.400	0.200
17.....	20 33 33.1	59 58 15.1	0.140	0.040	0.040	0.040	1.100	0.900
20.....	20 33 33.5	59 58 15.9	0.130	0.050	0.030	0.030	1.300	1.100
22.....	20 33 34.5	59 59 12.6	0.410	0.050	0.130	0.030	0.900	0.200
23.....	20 33 36.1	59 54 28.7	0.350	0.040	0.180	0.060	0.500	0.300
25.....	20 33 37.1	59 58 26.2	0.160	0.040	0.030	0.030	1.500	1.100
26.....	20 33 38.3	59 58 22.0	0.870	0.060	0.510	0.040	0.400	0.100
34.....	20 33 44.6	59 59 34.5	0.130	0.050	0.020	0.020	1.300	0.900
35.....	20 33 45.1	59 57 39.9	0.230	0.030	0.070	0.030	0.900	0.300
40.....	20 33 46.0	59 58 24.1	0.100	0.040	0.010	0.020	1.600	1.400
43.....	20 33 46.6	59 57 41.3	0.090	0.040	0.020	0.020	1.200	0.800
45.....	20 33 47.0	59 58 47.1	0.320	0.060	0.120	0.030	0.800	0.300
48.....	20 33 47.9	59 59 55.8	0.430	0.060	0.280	0.030	0.400	0.100
49.....	20 33 47.9	59 58 31.9	0.130	0.050	0.030	0.020	1.100	0.600
51.....	20 33 48.2	59 57 14.4	0.410	0.080	0.150	0.030	0.800	0.200
53.....	20 33 48.3	59 58 29.1	0.100	0.040	0.030	0.020	0.900	0.700
54.....	20 33 48.3	59 59 09.2	0.280	0.090	0.080	0.030	1.000	0.400
60.....	20 33 49.6	59 57 29.3	0.150	0.030	0.080	0.020	0.500	0.300
63.....	20 33 50.0	59 58 22.9	0.320	0.050	0.070	0.030	1.200	0.300
66.....	20 33 50.2	59 56 50.6	0.250	0.030	0.050	0.020	1.200	0.300
68.....	20 33 50.5	59 56 48.8	0.170	0.030	0.030	0.020	1.400	0.700
69.....	20 33 50.6	59 58 53.8	0.640	0.170	0.360	0.090	0.500	0.300
75.....	20 33 51.3	59 59 02.0	0.190	0.050	0.010	0.020	2.100	1.200
83.....	20 33 55.6	60 00 26.7	0.510	0.060	0.270	0.060	0.500	0.200
84.....	20 33 56.0	59 54 12.9	0.380	0.040	0.090	0.050	1.100	0.500
85.....	20 33 57.7	60 01 05.2	1.590	0.050	0.820	0.040	0.500	0.100
88.....	20 34 00.9	59 59 28.8	0.110	0.030	0.040	0.020	0.900	0.500
89.....	20 34 01.1	60 00 29.2	0.360	0.060	0.130	0.030	0.800	0.200
95.....	20 34 02.6	60 00 41.5	0.140	0.040	0.050	0.040	0.900	0.700
99.....	20 34 03.6	60 00 45.3	0.270	0.060	0.150	0.040	0.500	0.300
101	20 34 05.0	60 00 47.3	0.700	0.060	0.320	0.030	0.600	0.100
107	20 34 08.3	59 58 46.0	0.200	0.030	0.090	0.040	0.600	0.300
118	20 34 22.0	59 59 31.2	2.870	0.080	1.850	0.100	0.400	0.100

NOTE.—Units of right ascension are hours, minutes, and seconds, and units of declination are degrees, arcminutes, and arcseconds.

but we assume a value of ~ 5.1 Mpc (de Vaucouleurs 1979) in comparing to other studies in which this value was also assumed.

The SNRs in this sample were identified in a VLA survey of NGC 6946 at 6 and 20 cm (for observing parameters see Table 1), as described in Lacey et al. (1997). The candidates were selected on the basis of having a nonthermal spectral index α (where $S_\nu \propto \nu^{-\alpha}$) and are listed in Table 2. The columns for Table 2 are as follows: column (1) is the SNR source number from column (1) in Table 2 of Lacey et al. (1997); columns (2) and (3) are the B1950 right ascension and declination coordinates, respectively; columns (4)–(7) are the flux density and the standard deviation at 20 and 6 cm, respectively; and columns (8) and (9) are the spectral index and the standard deviation, respectively. Background radio sources (radio galaxies and quasars seen through the disc of NGC 6946) were eliminated from the sample by requiring that the radio source have associated compact Hα emission, assumed to originate from the SNR on the basis of its compact, pointlike morphology. At the distance of NGC 6946, $1'' \approx 20$ pc; thus, the SNRs are expected to appear pointlike in the optical images. The occasional coincidence of a nonthermal radio source with a compact H II region cannot be ruled out; however, a compact nonthermal source associated with Hα emission is not likely to be a background source because radio galaxies and quasars have their Hα emission shifted out of the filter response, which was tuned for the rest frame of NGC 6946.

Based on our earlier study of M33, we expect that most of the 35 radio-selected SNRs identified in NGC 6946 are middle-aged remnants in the adiabatic phase of expansion with lifetimes of 10^4 yr rather than in the free expansion phase, which is predicted to last at most a few thousand years (see Duric et al. 1995; Gordon et al. 1998, 1999). The historical supernova SN 1968D was detected at both 6 and 20 cm in this VLA survey, although no detectable discrete Hα emission was identified by us or by Matonick & Fesen (1997) using different Hα data. Because of the young age of SN 1968D, we do not include it in the sample of SNRs in NGC 6946.

An unpublished Hα image of NGC 6946 was obtained from W. P. Blair. The image was taken on 1990 September 28 at the 4 m Kitt Peak Telescope with an Hα filter. The image was reduced using normal procedures in IRAF.

Positions of Hα sources were determined with the STSDAS package in IRAF using positions of stars from the Guide Star Catalog.[3] The resolution of the Hα image is $\sim 1''$, approximately the same resolution as the radio image. The Hα image has well-defined spiral arms and many complex H II regions as well as pronounced Hα emission in the nucleus due to starburst activity. The radio and optical data sets are well matched for the purposes of this study.

Matonick & Fesen (1997) performed an optical search for SNRs in NGC 6946 using imaging techniques and the S II/Hα ratio to identify SNRs. They identified 27 SNRs with this method. In this paper we use their optically identified SNR sample to compare with the radio-selected sample presented in this paper.

[3] The Guide Star Catalog was produced at the Space Telescope Science Institute under a US Government grant. These data are based on photographic data obtained using the Oschin Schmidt Telescope (operated by the California Institute of Technology and Palomar Observatory) on Palomar Mountain and the UK Schmidt Telescope (operated by the Royal Observatory Edinburgh, with funding from the UK Science and Engineering Research Council [later the UK Particle Physics and Astronomy Research Council] until 1988 June and thereafter by the Anglo-Australian Observatory).

3. THE LUMINOSITY FUNCTION OF THE RADIO SNRS IN NGC 6946

The luminosity function of the 35 radio-selected SNRs in NGC 6946 is shown in Figure 1. For comparison, the luminosity function of radio SNRs in M33 (Duric et al. 1995) is also plotted, in which the flux densities of SNRs in M33 are scaled to the distance of NGC 6946. Both luminosity functions are incomplete at lower surface brightnesses, as expected. The radio continuum luminosities of the radio-selected SNRs in NGC 6946 vary from 0.1 to 2 times the luminosity of Cassiopeia A, suggesting that they are comparable to the brighter SNRs in our Galaxy. A comparison with the SNRs in M33 (Fig. 1) shows that the SNRs in NGC 6946 are on average 10 times more luminous than those in M33 (assuming distances of 5.1 Mpc and 840 kpc for NGC 6946 and M33, respectively).

NGC 6946 is thought to have roughly the same size and mass as our own Galaxy. The luminosity function of NGC

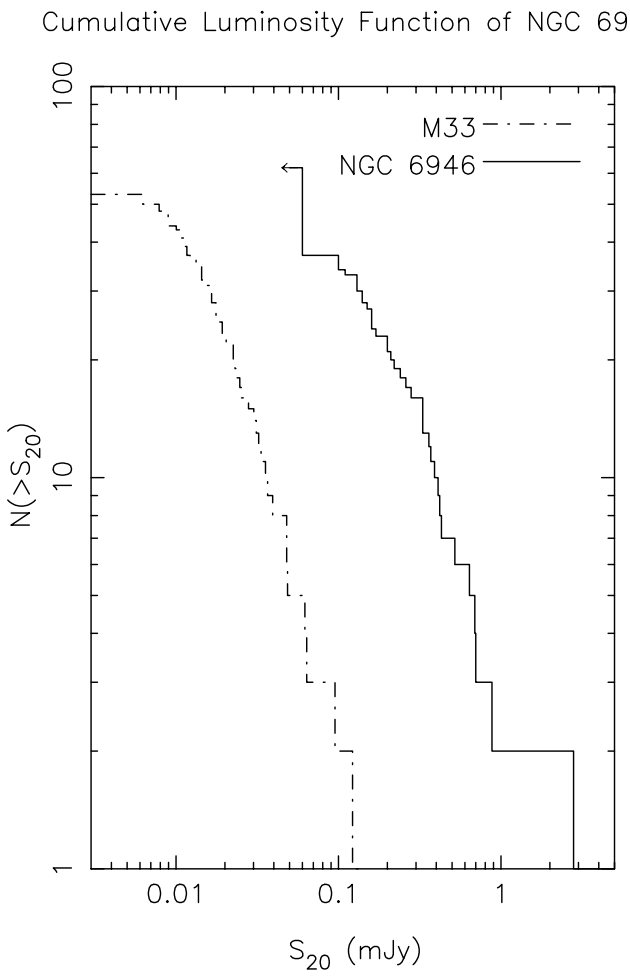

FIG. 1.—Luminosity function of the SNRs in NGC 6946 (*solid line*) plotted with the luminosity function of M33 (*dot-dashed line*; Gordon et al. 1999), which is scaled to the distance of NGC 6946. The SNRs in NGC 6946 are clearly more luminous than the SNRs in M33. An upper limit for the flux density of 25 optically selected SNRs in NGC 6946 is included in the luminosity function.

6946 is similar in shape to that of M33, although the SNRs in NGC 6946 are consistently more luminous than those in M33. This may well be because of the greater mass and higher star formation rate in NGC 6946, leading to a greater steady state population of SNRs. The luminosity functions of both NGC 6946 and M33 have abrupt cutoffs at lower flux densities because of the surface brightness limits of the respective radio surveys.

4. PROGENITOR STARS OF THE RADIO-SELECTED SNRS

In order to investigate which type of SNe is responsible for radio-selected SNRs, and therefore the CR electron acceleration, we have plotted the positions of the radio-selected SNRs on an Hα image of similar resolution and compared the nonthermal radio emission with the Hα emission. Figure 2 illustrates the positions of the radio-selected SNRs relative to the Hα arms in NGC 6946. The spiral arms were defined in Matonick & Fesen (1997), in which they used an optical continuum image of NGC 6946 that best showed the spiral arm structure and traced the spiral arms along the peak surface brightness ridge lines of each arm (see Fig. 3). We used the same width of the spiral arms, 25″, that Matonick & Fesen (1997) used in order to compare directly our statistical properties with their cited values. Matonick & Fesen (1997) arrived at the value of 25″ based on the average value of the widths of spiral arms in five nearby galaxies, including NGC 6946. The definition of the extent of the spiral arms by Matonick & Fesen (1997) depended on their Hα image; deeper Hα images (see Ferguson et al. 1998) show much more extensive Hα arms.

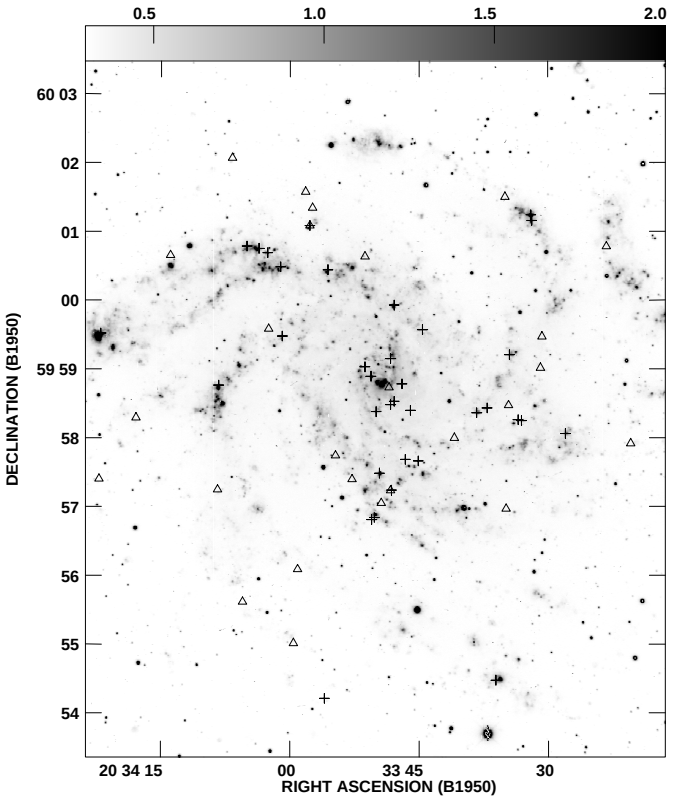

FIG. 2.—Kitt Peak 4 m Hα image of NGC 6946 with SNR positions overlaid. The crosses are the radio-selected SNRs (Lacey & Duric 1997), and the triangles are the optically selected SNRs (Matonick & Fesen 1997). The radio sources generally lie in the spiral arms or near H II regions. The optical SNRs tend to lie in the interarm regions or along the edges of the spiral arms. Hα image courtesy of W. P. Blair.

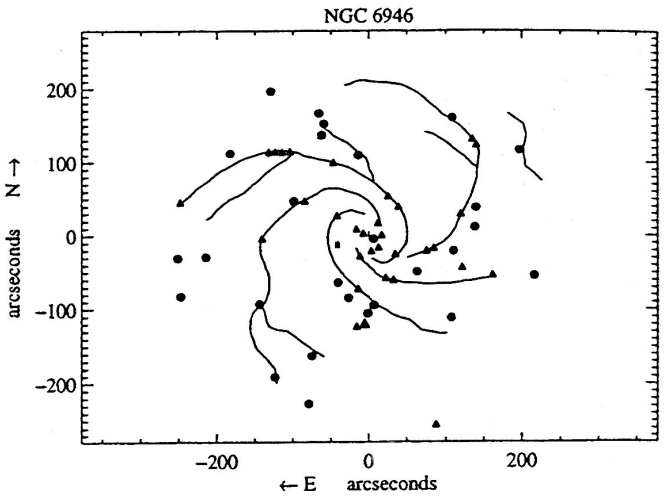

FIG. 3.—Spiral arms of NGC 6946 traced out with the positions of the 25 optically selected SNRs, represented by circles, with 35 radio-selected SNRs overlaid. The locations of the majority of the radio-selected SNRs are on the spiral arms, whereas the majority of the optically selected SNRs are on the edges of the arms or in the interarm regions. This figure is adapted from Matonick & Fesen (1997).

A random population of 40 sources was generated to compare with the optical and radio-selected samples. The random sources were generated in the same 9′ × 9′ square that was used to identify radio SNR candidates. Table 3 presents the positions of the radio-selected SNRs, optically selected SNRs, and random sources along with the distance to the nearest H II region and the position of the source relative to the nearest spiral arm. The radio-selected SNRs are identified by the catalog source number from Table 2 of Lacey et al. (1997), and the optically selected SNRs are identified by "MF" followed by their identification number given in Table 8 of Matonick & Fesen (1997) to designate the optically selected sample of SNRs. The location of each SNR is labeled "arm" if the SNR's position is coincident with an optical spiral arm, "arm edge" if the SNR's position is on the edge of a spiral arm within 25″ of the spiral arm but not associated with the Hα emission of the arm, "interarm" if the SNR's position is in between the optical spiral arms, and "nucleus" if the SNR is associated with the nucleus. Inspection of Table 3 shows that the radio-selected SNRs tend to be found in the arms, while the optically selected SNRs tend to be found away from the arms.

Table 4 tallies the number of sources in the various regions of NGC 6946, including the inner region of NGC 6946 (<3′) and the outer region (>3′). It is interesting to note that both the optical and random samples have large numbers of sources occurring in the interarm and outer regions of the galaxy compared to the radio sample. The large number of random sources in the outer part of NGC 6946 is due in part to the larger physical area covered in the 9′ × 9′ square field of view larger than the radius of 3′. It is interesting to note that the radio-selected sample of SNRs has roughly equal numbers of inner and outer SNRs.

There are a total of 30 radio-selected SNRs that lie on the arms or in the central part of the galaxy. Two of these are on the edge of a spiral arm. Only five radio-selected SNRs are not directly associated with the arms as defined by Matonick & Fesen (1997).

TABLE 3

POSITIONS AND RELATIVE DISTANCES OF THE RADIO AND OPTICALLY SELECTED SNRs AND THE RANDOM SOURCES IN NGC 6946

ID Number	R.A. (B1950)	Decl. (B1950)	Distance[a] (arcsec)	Position on Spiral Arm
8	20 33 28.0	59 58 03.8	5.4	Arm
12	20 33 31.9	60 01 09.7	0.0	Arm
13	20 33 32.0	60 01 14.6	0.0	Arm
17	20 33 33.1	59 58 15.1	0.0	Interarm
20	20 33 33.5	59 58 15.9	3.6	Interarm
22	20 33 34.5	59 59 12.6	3.6	Arm
23	20 33 36.1	59 54 28.7	3.6	Interarm
25	20 33 37.1	59 58 26.2	7.2	Arm
26	20 33 38.3	59 58 22.0	0.0	Arm
34	20 33 44.6	59 59 34.5	5.4	Arm
35	20 33 45.1	59 57 39.9	1.8	Arm
40	20 33 46.0	59 58 24.1	7.2	Arm
43	20 33 46.6	59 57 41.3	9.0	Arm
45	20 33 47.0	59 58 47.1	5.4	Nucleus
48	20 33 47.9	59 59 55.8	0.0	Arm
49	20 33 47.9	59 58 31.9	3.6	Nucleus
51 (MF9)	20 33 48.2	59 57 14.4	7.2	Arm
53	20 33 48.3	59 58 29.1	7.2	Nucleus
54	20 33 48.3	59 59 09.2	1.8	Arm
60	20 33 49.6	59 57 29.3	0.0	Arm
63	20 33 50.0	59 58 22.9	1.8	Arm
66	20 33 50.2	59 56 50.6	1.8	Arm
68	20 33 50.5	59 56 48.8	3.6	Arm edge
69	20 33 50.6	59 58 53.8	0.0	Arm edge
75	20 33 51.3	59 59 02.0	3.6	Nucleus
83	20 33 55.6	60 00 26.7	1.8	Arm
84	20 33 56.0	59 54 12.9	14.4	Interarm
85 (MF16)...	20 33 57.7	60 01 05.0	0.0	Interarm
88	20 34 00.9	59 59 28.8	1.8	Arm
89	20 34 01.1	60 00 29.2	0.0	Arm
95	20 34 02.6	60 00 41.5	0.0	Arm
99	20 34 03.6	60 00 45.3	0.0	Arm
101.....	20 34 05.0	60 00 47.3	0.0	Arm
107.....	20 34 08.3	59 58 46.0	0.0	Arm
118.....	20 34 22.0	59 59 31.2	0.0	Arm
MF1	20 33 20.4	59 57 55.1	5.4	Interarm
MF2	20 33 23.2	60 00 47.0	0.0	Arm edge
MF3	20 33 30.7	59 59 28.4	12.6	Interarm
MF4	20 33 30.9	59 59 01.1	7.2	Interarm
MF5	20 33 34.6	59 58 28.4	18.0	Interarm
MF6	20 33 35.0	60 01 30.2	1.8	Arm edge
MF7	20 33 34.9	59 56 58.2	7.2	Interarm
MF8	20 33 40.9	59 57 60.0	7.2	Interarm
MF9	20 33 48.3	59 57 14.2	7.2	Arm
MF10.....	20 33 48.5	59 58 44.0	0.0	Nucleus
MF11.....	20 33 49.4	59 57 03.2	5.4	Arm edge
MF12.....	20 33 51.3	60 00 38.3	1.8	Arm edge
MF13.....	20 33 52.8	59 57 23.9	7.2	Arm edge
MF14.....	20 33 54.7	59 57 44.6	5.4	Arm edge
MF15.....	20 33 57.4	60 01 20.6	12.6	Interarm
MF16.....	20 33 57.7	60 01 05.2	0.0	Interarm
MF17.....	20 33 58.2	60 01 34.7	7.2	Interarm
MF18.....	20 33 59.1	59 56 05.5	18.0	Arm edge
MF19.....	20 33 59.6	59 55 01.0	7.2	Interarm
MF20.....	20 34 02.5	59 59 35.1	10.8	Arm edge
MF21.....	20 34 05.5	59 55 37.0	14.4	Interarm
MF22.....	20 34 06.7	60 02 04.1	7.2	Interarm
MF23.....	20 34 08.4	59 57 15.0	5.4	Interarm
MF24.....	20 34 13.9	60 00 39.3	7.2	Interarm
MF25.....	20 34 17.9	59 58 17.7	10.8	Interarm
MF26.....	20 34 22.2	59 57 24.2	18.0	Interarm
MF27.....	20 34 22.8	59 58 16.0	10.8	Interarm
Random Sources				
R1	20 33 11.1	60 02 07.3	18.0	Interarm
R2	20 33 13.7	59 54 57.3	21.6	Interarm
R3	20 33 15.3	59 54 40.9	3.6	Interarm
R4	20 33 17.8	60 01 00.8	7.2	Interarm
R5	20 33 19.1	60 01 53.4	25.2	Interarm
R6	20 33 21.1	59 58 10.3	5.4	Interarm
R7	20 33 21.8	59 55 51.9	18.0	Interarm
R8	20 33 22.6	59 55 36.8	7.2	Interarm
R9	20 33 22.9	59 57 12.3	7.2	Interarm
R10.....	20 33 23.0	59 58 20.8	7.2	Arm edge
R11.....	20 33 26.3	59 56 25.3	18.0	Interarm
R12.....	20 33 27.4	59 58 13.1	3.6	Arm
R13.....	20 33 29.2	59 59 32.4	14.4	Arm edge
R14.....	20 33 33.2	60 02 10.1	10.8	Interarm
R15.....	20 33 34.3	59 56 38.8	10.8	Interarm
R16.....	20 33 38.7	60 02 41.7	10.8	Interarm
R17.....	20 33 38.9	59 54 27.3	10.8	Interarm
R18.....	20 33 39.1	59 54 13.2	10.8	Interarm
R19.....	20 33 42.4	59 57 47.0	7.2	Arm
R20.....	20 33 44.6	59 57 43.2	7.2	Arm
R21.....	20 33 49.5	60 01 55.5	14.4	Arm edge
R22.....	20 33 49.6	60 01 00.4	10.8	Arm edge
R23.....	20 33 51.7	60 03 27.7	18.0	Interarm
R24.....	20 33 54.6	59 59 43.1	18.0	Arm
R25.....	20 33 56.2	59 58 59.2	7.2	Arm
R26.....	20 33 57.5	59 59 51.7	3.6	Nucleus
R27.....	20 34 00.7	59 57 42.8	10.8	Interarm
R28.....	20 34 01.4	59 56 19.1	7.2	Arm
R29.....	20 34 01.4	59 59 03.8	3.6	Arm edge
R30.....	20 34 03.7	60 01 44.5	21.6	Interarm
R31.....	20 34 05.3	60 02 50.3	1.8	Interarm
R32.....	20 34 05.4	60 03 03.9	7.2	Interarm
R33.....	20 34 09.2	59 55 10.6	10.8	Interarm
R34.....	20 34 09.3	59 58 36.4	1.1	Arm
R35.....	20 34 15.5	59 54 46.0	10.8	Interarm
R36.....	20 34 17.3	59 58 08.7	3.6	Interarm
R37.....	20 34 18.3	59 57 12.1	3.6	Interarm
R38.....	20 34 19.9	60 02 52.3	14.4	Interarm
R39.....	20 34 21.5	59 54 49.3	7.2	Interarm
R40.....	20 34 20.4	60 01:56.6	7.2	Interarm

NOTE.—Units of right ascension are hours, minutes, and seconds, and units of declination are degrees, arcminutes, and arcseconds.

[a] Distance in from the source to the nearest H II Region.

Closer inspection of the Hα image from Blair and a very deep Hα image from Ferguson et al. (1998) reveals that the spiral arms are more extensive in length than indicated by Matonick & Fesen (1997). Three of the interarm radio-selected SNRs, including SNR 23, which is 120″ from the nearest spiral arm as defined by Matonick & Fesen (1997), can be identified with the fainter, more extensive Hα arms. Thus, most of the radio-selected SNRs are associated with the spiral arms or nucleus of NGC 6946 and are never found more than 20″($\approx$400 pc) from the ridge lines (centers) of the spiral arms. Of the optically identified SNRs, two are associated with an arm or the central region, eight are just beyond the outer edges of the spiral arms, and 17 are not associated with the spiral arms (more than 400 pc from the ridge lines). Matonick & Fesen (1997) found that their sample of optically selected SNRs was not statistically associated with the spiral arms, which is in agreement with our analysis. The basic conclusion is that 83% of the radio-

TABLE 4

NUMBERS OF SNRs LOCATED IN VARIOUS REGIONS OF NGC 6946

Population	Spiral Arm	Spiral Arm Edge	Nucleus	Interarm	Inner Galaxy	Outer Galaxy
Radio.....	25	2	4	6	20	17
Optical	1	8	1	17	7	20
Random.....	7	5	1	27	6	34

selected SNRs lie on the spiral arms or in the nucleus, while 66% of the optically identified SNRs lie outside the arms.

Comparison of the radio and optically selected samples of SNRs indicates that two SNRs are common to both data sets. SNR 85 corresponds to the optical SNR MF16, first discussed by Blair & Fesen (1994). SNR 85 is also an extremely luminous X-ray source (Schlegel 1994). Blair, Fesen, & Schlegel (2001) reported evidence that this SNR is actually two interacting SNRs from *Hubble Space Telescope* observations, which may account for the high X-ray, radio, and optical luminosities.

Further high-resolution observations are needed to determine the exact nature of this luminous source. The other correspondence is the radio-emitting SNR 51 with SNR MF9, located in a spiral arm.

4.1. *Statistical Test of the Parent Distributions of SNRs*

The Kolmogorov-Smirnov (K-S) test was used to compare the optically and radio-selected SNRs with H II regions and the random source population. The K-S test was used since the true underlying distribution of SNRs is not known and the K-S test is sensitive as to whether two populations have the same parent distribution. The distances of the radio, optical, and random sources to the nearest H II region were measured, and then the distributions of distances were used in several K-S tests (see Table 5). The results of the K-S tests confirm our conclusion that the radio SNRs likely are associated with the H II and star formation regions in NGC 6946. The optical SNRs are probably not associated with H II regions, which is the same conclusion that Matonick & Fesen (1997) reached.

Another interesting result is that the inner (within 3′ of the nucleus) optically selected SNRs and random sources have a greater correlation with H II regions than the outer ($>3'$ of the nucleus) optical and randomly generated sources. This result is due to a bias in that the density of H II regions is large and the H II regions cover a large fraction of the area in the central part of NGC 6946; it is rare to find a random source that is not near an H II region in the central region of NGC 6946. This also biases the K-S test of radio-selected SNRs with optically selected SNRs. The inner optical SNR distribution appears possibly to be correlated with the inner radio SNR distribution, but this is not found in the outer SNR population. In fact, the inner radio SNRs also have a much higher probability ($P = 0.15$) in a K-S test to be correlated with the inner randomly generated sources. The inner random sources show a higher likelihood of correlation with H II regions, which is also a consequence of the high density of H II regions in the inner part of the galaxy. The statistical tests of all the SNRs in NGC 6946 and the outer SNR populations have greater significance in that they are less biased than the tests of the inner populations.

The segregation of the two samples of SNRs implies that strong selection effects play a major role in the identification of SNRs. The above results suggest that the radio-selected SNRs are more closely associated with star-forming regions and that, on average, these SNRs are evolving in denser environments relative to the optically selected SNRs. The arm/interarm segregation of the SNRs raises the further possibility that the two populations of SNRs may have evolved from different precursors, i.e., that

TABLE 5

KOLMOGOROV-SMIRNOV (K-S) PROBABILITY

Population[a]	Probability	Interpretation
	H II Regions	
Radio	9×10^{-7}	Radio SNRs associated with H II regions
Optical.....	0.40	Optical SNRs probably not associated with H II regions
	Inner (radius $<3'$) and Outer (radius $>3'$) SNRs with H II Regions	
Inner radio	2×10^{-5}	Inner radio SNRs associated with H II regions
Outer radio	8×10^{-6}	Outer radio SNRs associated with H II regions
Inner radio/Inner random.....	0.15	Ambiguous: Inner random sources are more correlated with H II regions because of the high density and large covering factor of H II regions in the inner part of the galaxy
Outer radio/Outer random.....	2×10^{-5}	Outer radio SNRs are associated with H II regions
Inner optical	0.003	Inner optical SNRs possible associated with H II regions
Outer optical.....	0.80	Outer optical SNRs probably not associated with H II regions
	Radio and Optical SNR Comparison	
Radio/Optical.....	2×10^{-4}	Radio and optical SNRs possibly have a similar parent distribution

[a] Radio indicates the radio-selected sample presented in this paper and optical indicates the sample from Matonick & Fesen 1997. The distributions listed in this column are compared in a K-S test with 40 randomly generated sources unless specifically noted.

the interarm SNRs arose from Type Ia SNe and the arm SNRs from Type II/Ib/Ic SNe.

4.2. *Progenitor Populations of SNRs in NGC 6946*

Type II/Ib/Ic SNe are believed to have massive, Population I progenitors. Because the progenitors are short-lived (10^6 yr) massive stars, Type II/Ib/Ic SNe are expected to occur near their birth sites in the star-forming regions since they cannot disperse far from their birth sites because of their short lives. On the other hand, Type Ia SNe are thought to arise from white dwarfs in binary star systems. White dwarfs are old, evolved stars that have had significant amounts of time to disperse from their birth sites, as evidenced by their generally broader distribution in disk galaxies relative to the Population I stars. Consequently, it is expected that, on average, white dwarfs should be found in lower density environments compared to the Population I stars and their remnants. Thus, Type II/Ib/Ic SNe generally occur in or near star-forming regions where the densities are, on average, higher.

We now explore the possibility that the arm SNRs arise from Population I precursors and that the interarm SNRs have a Population II origin. Of the 27 optically selected SNRs, 17 are clearly interarm objects. Of the 35 radio-selected SNRs, 30 (86%) are clearly in or near the arms. Thus, there are a total of 40 SNRs associated with the arms and 22 SNRs associated with the interarm regions. Assuming that this is entirely due to precursor differences, then roughly one-third of the detected SNRs have Population II stellar precursors (i.e., they are Type Ia SNe remnants), while two-thirds have Population I stellar precursors (i.e., they are Type II or Ib/c SNe remnants). It is interesting to compare this ratio to that of the frequency ratios of various types of SNe.

Chu & Kennicutt (1988) determined that the minimum ratio between SNRs with Population I to Population II precursors in the Large Magellanic Cloud (LMC) was at least 2.7–4.5:1. Chu & Kennicutt (1988) also believe that they have missed many of the optical Population I SNRs because of obscuration in H II regions and other dense star-forming areas in the LMC. The data from NGC 6946 also suggest that many optically selected SNRs with Population I precursors are missing. The number of radio SNRs with Population I precursors is also expected to rise with more sensitive radio surveys. Many nonthermal sources in NGC 6946 were not included in this study because of weak or nondetections of 6 cm emission, which resulted in poorly defined spectral indices and thus were not included as SNRs even though they are certainly nonthermal.

From optical SNe surveys, Tammann, Löffler, & Schröder (1994) estimated that for an Sc spiral galaxy, the massive star progenitor (Type II + Ib/c) contribution to the total number of SNe contribution could be as large as 91%. There is therefore general agreement with our measured ratio of types in the sense that the majority of the SNRs may have massive stellar precursors. However, the SNe frequency statistics predict a smaller percentage of Type Ia SNe relative to our interpretation of the observed SNR statistics. We speculate that this excess can be explained by the fact that the two populations of SNRs are selected by different techniques and are therefore subject to different selection effects. The radio-selected sample is limited by the sensitivity of the radio observations and the ability to separate thermal and nonthermal emission, while the optical sample, with similar angular resolution, is limited by the ability to discern between photoionized and shock-excited emission. The optically selected sample appears to have missed many SNRs located in the arms of NGC 6946. We believe that this bias is the result of the confusing effect of Hα emission from the numerous H II regions in the spiral arms (T. P. Pannuti et al. 2001, in preparation). Although our assumptions need confirmation, it does seem that our data are consistent with a scenario in which the SNRs arise from two distinct populations of stellar precursors.

The association of radio-emitting SNRs with Population I stars has interesting implications for cosmic-ray theory. Since we expect cosmic ray–producing SNRs to be radio sources, the implication is that the progenitor stars of radio-bright SNRs are Population I stars. The association is not surprising, but this evidence is the first to directly demonstrate that cosmic ray–producing SNRs result from massive short-lived Population I stars.

We note that even if the optically and radio selected SNRs do not represent two distinct populations with different stellar origins, the two samples are distinct in terms of the environment in which the SNRs are found. The average gas densities in the spiral arm can often be 3–4 times greater than in the interarm regions (see, e.g., Taylor & Cordes 1993). It is expected that most Type Ia SNe should have lower levels of radio emission because of lower ambient magnetic field strengths and weaker shock/ISM interactions. These ideas are consistent with our findings that radio-bright SNRs are found preferentially in the spiral arms. The dependence of cosmic-ray production on the environment is discussed in the next section, in which we place the above discussions on a more quantitative footing.

5. ENVIRONMENTAL EFFECTS ON RADIO EMISSIVITY

The primary result from the previous section suggests that the cosmic ray–producing SNRs lie in the spiral arms of NGC 6946. This scenario can be quantified by examining the physical processes responsible. The broader question that arises is whether the marked difference in the properties of the arm and interarm SNRs is the result of environmental factors only or whether there is a real difference in the capabilities of the two SNR populations to accelerate cosmic rays. In other words, are the differences in radio properties the result of shock-driven modulation of ambient cosmic rays and magnetic fields or does the efficiency of active particle acceleration account for these differences?

5.1. *Compression*

There are essentially two physical possibilities to explain the preferred location of radio-bright SNRs in the arms. The first possibility is that the radio-selected SNRs are bright radio sources because the radio-selected SNRs produce a greater number of relativistic electrons through particle acceleration. This straightforward explanation accounts for the empirical result from the previous section. However, the second possibility is that the radio-bright SNRs are compressing preexisting cosmic rays and magnetic fields, thereby boosting synchrotron emission without substantially increasing the production of accelerated particles. This second possibility implies that the SNRs on the spiral arms are brighter in the radio because of their location on the spiral arms, where the density of cosmic rays and strength of the magnetic fields are greater than in the interarm region. We have devised a test to determine

whether compression of preexisting cosmic rays is responsible for the differences in radio emissivity of SNRs in the arm and interarm regions or whether the differences are the result of active particle acceleration.

5.1.1. *Adiabatic Compression: Effect on the Total Nonthermal Energy*

We now consider the effects of simple shock compression and investigate whether compression alone accounts for the radio emission observed from the SNRs in NGC 6946. We first examine the energy associated with maximum adiabatic compression of the ambient magnetic field in the absence of particle acceleration and any other magnetic field amplification. The total nonthermal energy is defined as

$$U_{\rm total} = U_B + U_{\rm CR} . \tag{1}$$

The magnetic field energy is given by (Pacholczyk 1970)

$$U_B = \frac{B^2}{8\pi} \phi V \text{ ergs}, \tag{2}$$

where V is the volume of the SNR and ϕ is the filling factor (fraction of the volume of the SNR that is occupied by the magnetic field). The filling factor for Galactic remnants in the adiabatic phase of expansion, where the shell can be resolved, has been generally determined to be $\phi \sim \frac{1}{4}$ (Reynolds 1988).

Assume that the ambient, homogeneous magnetic field is B_0. The maximum compression for an adiabatic shock in an ideal gas is a factor of 4. The magnetic field strength increases because of the adiabatic compression, but only the component of the field that is parallel to the shock is amplified. Thus, an azimuthal average around the SNR would yield an effective compression factor of roughly 2. Let us now consider a specific example.

Let the radius of a remnant be $r = 10$ pc and let the ambient magnetic field be $B_0 = 12$ μJy, which is the average interstellar magnetic field in the disk of NGC 6946 (Ehle & Beck 1993). The resulting magnetic field energy is $U_B \sim 2 \times 10^{47}$ ergs.

If we assume equipartition between the disk magnetic field energy and the disk cosmic rays, equation (1) becomes

$$U_{\rm total} = U_B + U_{\rm CR} \simeq 2U_B = 4 \times 10^{47} \text{ ergs}. \tag{3}$$

This estimate for $U_{\rm total}$ is several orders of magnitude below the kinetic energy of the SNR, assumed to be $\sim 10^{51}$ ergs. If equipartition does not hold, then the magnetic field energy or the cosmic-ray energy (but not both) could be higher, increasing the total nonthermal energy. Substantial increases in either the disk magnetic field or the disk cosmic-ray energies would be needed to change our conclusion. No evidence for such increases exists.

If we now consider a much larger SNR, with a radius of 40 pc, then $U_{\rm total}$ increases to $\sim 2 \times 10^{49}$ ergs, which is still 2 orders of magnitude below the kinetic energy of the remnant but closer to estimated minimum nonthermal energies of SNRs (Duric et al. 1995). On the basis of this argument, only the largest SNRs could produce the needed nonthermal energy through shock compression alone.

5.1.2. *Boosting of Radio Surface Brightness*

Another test of the compression model relates to the ability of shock compression to account for the observed radio surface brightness of an SNR. We investigate whether boosting of the surface brightness by compression can be responsible for the differences in radio properties of the two samples of SNRs.

At a given frequency, the radio flux density depends on the strength of the magnetic field B and the density of the cosmic-ray electrons N such that

$$S \propto NB^{1+\alpha} \tag{4}$$

according to synchrotron theory.

Consider an ambient medium denoted with subscript "0" and a compressed medium with an increased cosmic-ray density, denoted by subscript "1":

$$\frac{S_1}{S_0} = \frac{N_1 B_1^{1+\alpha_1}}{N_0 B_0^{1+\alpha_0}} . \tag{5}$$

The spectral index of the disk emission in NGC 6946 is $\alpha = 0.8$. Assuming $N_1 = 4N_0$ for maximum adiabatic compression of the cosmic rays and $B_1 = 2B_0$ for maximum adiabatic compression of B, then

$$\frac{S_1}{S_0} = 14 . \tag{6}$$

Let the radius of the remnant be 10 pc. Using the measurement by White & Becker (1992) of the 1.4 GHz total integrated flux density of NGC 6946 of $S_0 = 1.5$ Jy and a diameter of 10′, the flux density per square arcsecond, S_0 arcsec^{-2}, can be crudely estimated as

$$S_0 \text{ arcsec}^{-2} = 4 \times 10^{-3} \text{ mJy arcsec}^{-2} . \tag{7}$$

Applying equation (6), the typical emissivity in compressed regions (the SNRs) should be $S_1 = 0.05$ mJy arcsec^{-2}. As Table 2 indicates, this value is less than most of the measured values of SNRs from NGC 6946. The total integrated flux density includes the nuclear component of NGC 6946 as well. Removing the $\sim$300 mJy nuclear component from the total integrated flux density leads to a smaller S_1 and therefore to greater deviations from the observed SNR surface brightnesses. Furthermore, we find no evidence that SNRs are brighter radio sources near the nucleus, where the ambient CR density is greater. Such a correlation would be expected if the SNRs were simply compressing the ISM of NGC 6946.

While adiabatic compression of magnetic fields and surface brightnesses can explain the low flux density end of the radio-selected SNR sample observed in NGC 6946, it cannot explain the higher end. Adiabatic compression has a role in the production of radio emission in SNRs, but it cannot be solely responsible for all of the observed radio emission from SNRs in NGC 6946. This conclusion agrees with work done on individual Galactic remnants such as Tycho (Reynolds 1988), Cassiopeia A (Anderson et al. 1991), and W49B (Moffett & Reynolds 1994), in which adiabatic compression alone could not explain the observed flux densities of the individual remnants.

5.2. *Equipartition*

Under the assumption of equipartition, the minimum energy of a radio source can be calculated. The minimum energy density of a remnant assuming equipartition can be calculated directly (Pacholczyk 1970):

$$U_{\rm min} = c_{13}(1+\eta)^{4/7} \phi^{\frac{3}{7}} R^{-6/7} L^{4/7} , \tag{8}$$

where η is the ratio of protons to electrons at a given energy, ϕ is the filling factor of the volume, here assumed to be $\phi \simeq 0.25$, which is typical for an adiabatic remnant shell remnant, R is the radius, L is the luminosity, and c_{13}, which is weakly dependent on α, is defined in Pacholczyk (1970). The minimum energy is weakly dependent on η and ϕ and is strongly dependent on the radius R of the emitting region.

The minimum energy $U_{\rm min}$ was calculated for all of the detected radio-selected SNRs in NGC 6946. A diameter, $D = 20$ pc, was assumed for each remnant; most radio-emitting remnants have radii that range from 10 to 40 pc (see, e.g., the M33 study of Duric et al. 1995). The expected dispersion in the calculated $U_{\rm min}$, resulting from our assumption of the diameter, has been incorporated into the quoted uncertainty. The results are shown in Table 6. The median value for $U_{\rm min}$ is $\langle U_{\rm min} \rangle = 2.2(\pm 1.0) \times 10^{50}$ ergs, ≈ 2 orders of magnitude higher than can be achieved by compression alone.

If the cosmic rays and magnetic fields of the SNRs are not in equipartition (likely to be the case), the total nonthermal energy increases strongly with departure from equipartition, thereby increasing the disparity between the predictions of adiabatic compression and the empirically determined nonthermal energies. In summary, it is evident that compression alone fails to account for the radio properties of SNRs on two counts: the minimum energies of the SNRs in our sample and the observed radio luminosities. In the next section we examine the effects of particle acceleration on the radio flux densities.

TABLE 6

MINIMUM NONTHERMAL ENERGIES FOR 35 RADIO-SELECTED SNRs

Number	S_{20} (mJy)	B (G)	$U_{\rm min}$ (ergs)	Luminosity (ergs s^{-1})
8	0.20	1.9E−04	1.1E50	2.5E35
12	0.18	1.8E−04	1.1E50	1.8E35
13	0.63	2.6E−04	2.1E50	9.9E35
17	0.14	2.4E−04	1.8E50	1.0E35
20	0.13	2.9E−04	2.6E50	1.3E35
22	0.41	2.7E−04	2.3E50	2.8E35
23	0.35	2.2E−04	1.5E50	4.4E35
25	0.16	3.8E−04	4.5E50	2.7E35
26	0.87	2.8E−04	2.5E50	1.4E36
34	0.13	2.9E−04	2.6E50	1.3E35
35	0.23	2.3E−04	1.7E50	1.5E35
40	0.10	3.7E−04	4.3E50	2.3E35
43	0.09	2.3E−04	1.7E50	7.4E34
45	0.32	2.4E−04	1.8E50	2.3E35
48	0.43	2.3E−04	1.7E50	6.7E35
49	0.13	2.3E−04	1.7E50	9.3E34
51	0.41	2.6E−04	2.0E50	3.0E35
53	0.10	1.8E−04	1.0E50	6.7E34
54	0.28	2.6E−04	2.0E50	1.9E35
60	0.15	1.7E−04	9.1E49	1.9E35
63	0.32	3.3E−04	3.5E50	2.6E35
66	0.25	3.1E−04	3.0E50	2.1E35
68	0.17	3.4E−04	3.7E50	2.2E35
69	0.64	2.6E−04	2.1E50	8.0E35
75	0.19	8.1E−04	2.1E51	2.9E36
83	0.51	2.4E−04	1.8E50	6.4E35
84	0.38	3.2E−04	3.2E50	2.7E35
85	1.59	3.4E−04	3.5E50	2.0E36
88	0.11	1.9E−04	1.1E50	7.4E34
89	0.36	2.5E−04	1.9E50	2.6E35
95	0.14	2.0E−04	1.3E50	9.4E34
99	0.27	2.0E−04	1.3E50	3.4E35
101.....	0.70	2.7E−04	2.3E50	6.9E35
107.....	0.20	1.9E−04	1.1E50	2.0E35
118.....	2.87	4.0E−04	4.9E50	4.5E36

5.3. *Effect of Particle Acceleration*

Since simple adiabatic compression of the ambient medium does not provide sufficient increases in the radio surface brightnesses and nonthermal energies of SNRs, it is necessary to examine the effect of active particle acceleration. We proceed by examining the relationship between particle acceleration and the density of the ambient medium. A simple analytical relationship between these two quantities was formulated by Bell (1978a, 1978b), and we therefore proceed with that formulation because of its simplicity and ease of use.

For middle-aged remnants, such as were observed in M33 (Gordon 1993) and what we would expect to find in NGC 6946, the typical ages are 3000–5000 yr. These remnants would be in the adiabatic phase of their evolution. The radio emissivity ϵ of SNRs for a given shock velocity is described by Bell (1978b):

$$\epsilon(\nu) = \frac{g(\alpha)}{10^{-3}}\,\xi(\gamma)\,\frac{n}{\rm cm^{-3}}\left(\frac{\Psi_e}{4}\right)^{2\alpha} \times \left(\frac{v_s}{10^4\ \ {\rm km\ s^{-1}}}\right)^{4\alpha}\left(\frac{B}{10^{-4}\ \ {\rm G}}\right)^{\alpha+1} \times \left[1+\left(\frac{\Psi_e}{4}\right)^{-1}\left(\frac{v_s}{7000\ \ {\rm km\ s^{-1}}}\right)^{-2}\right]^{\alpha} \times \left(\frac{\nu}{\rm GHz}\right)^{-\alpha}\ \ {\rm W\ Hz^{-1}\ m^{-3}}\,, \tag{9}$$

$$g(\alpha) = 2.94 \times 10^{-34}(1.435 \times 10^5)^{0.75-\alpha}\,\frac{\alpha}{0.75}\,,$$

where $\Psi_e = 4$ is the injection energy in units of $(1/2m_p v_s^2)$ and $\phi_e = 10^{-3}$ is the injection rate of electrons as suggested by Bell (1978b), $\gamma = 2\alpha + 1$, $\xi(\gamma)$ is a slowly varying function of the spectral index tabulated in Ginzburg & Syrovatskii (1965), v_s is the shock velocity, n is the number density of *thermal* electrons in the ambient medium, and B is the magnetic field of the SNR. For a constant v_s and ν, the emissivity is strongly dependent on n and B.

The above equation can be used to devise a simple test. Let us consider an arm region a and an interarm region b and let v_s be constant for all SNRs. Then, according to equation (9),

$$\frac{\epsilon_a}{\epsilon_b} \propto \frac{n_a}{n_b}\frac{B_a^{1+\alpha}}{B_b^{1+\alpha}} \simeq \frac{n_a}{n_b}\left(\frac{B_a}{B_b}\right)^{1+\alpha}\,. \tag{10}$$

For $n_a/n_b \simeq 5$ (Ehle & Beck 1993), $B_a/B_b \simeq 2$, and $\alpha \simeq 0.75$,

$$\frac{\epsilon_a}{\epsilon_b} \approx 17\,. \tag{11}$$

The integrated flux density of the source is related to the emissivity by $S(t) = \epsilon(t)\Omega L \propto \epsilon(t)V(t)$, where S is the integrated flux density, Ω is the solid angle of the source, L is the path length of the radiating region, and V is the volume of the emitting region. From equation (11), one expects the

average difference in SNR flux densities between the arm and interarm regions to be ~ 17. Inspection of Table 6 shows that a factor of 30 easily accounts for the differences in the radio flux densities of the radio-selected samples of SNRs and the upper flux limit of the optically selected sample. Furthermore, since these ratios are determined in light of active particle acceleration, there is, in principle, no problem in satisfying the minimum nonthermal energy requirement to power the SNRs as radio sources. We caution that the relative arm/interarm values of gas density and magnetic field strengths are not well known. The above numbers are meant to illustrate simply that it is possible to account for the differences in the radio continuum properties of the two SNR populations by invoking plausible differences in the average environments of the two samples.

The above discussion represents an argument for explaining the differences in the radio fluxes of the two samples of SNRs. It is still necessary to show that the absolute flux densities of the SNRs can be explained by particle acceleration theory. We now demonstrate quantitatively that SNR flux densities can be accounted for by using the full form of equation (9) to calculate the SNR flux densities predicted by particle acceleration.

According to equation (9), the free parameters are n, the number density of *thermal* electrons in the ambient medium, B, the magnetic field of the SNR, α, the spectral index, and v_s, the shock velocity. First, let us calculate the expected flux density for a typical radio-selected SNR. For the arm region, assume the average ambient density is 1 cm^{-3} (Ehle & Beck 1993).

The maximum magnetic field that Ehle & Beck measured for NGC 6946 is ≈ 20 μG. We take this to be the arm field. If we further assume that SNR adiabatic shocks amplify this field by a factor of 4, the minimum SNR field must be ≈ 80 μG. We assume a shock velocity range of $v_s = 500$–7500 km s^{-1} and $\alpha = 0.75$. According to equation (9), the radio emissivity is sensitive to n, B, and v_s. By varying v_s, we predict that the range of observed flux densities should be $S = 0.05$–1 mJy. This range is consistent within the scope of our assumptions and with the observed flux densities of the radio-selected SNRs in NGC 6946 (see Table 2). The very bright SNRs, those with fluxes in excess of 1 mJy, are relatively rare and may be the result of interactions with higher than average ambient densities (high-density clumps are, in fact, expected in the arms).

In their study of NGC 6946, Ehle & Beck (1993) measured an arm-interarm density ratio of about 5 and average disk magnetic field of about 10 μG. Scaling from the number density used for the arm region, we adopt a value of $n = 0.2$ cm^{-3} for the interarm region and an interarm magnetic field of 10^{-4} G. With the same range of possible SNR shock velocities, we predict $S = 0.003$–0.06 mJy. It is interesting to note that this range of flux densities lies below our 3 σ detection limit, consistent with the radio properties of all but a handful of the optically selected SNRs.

The above represents a statistical argument for explaining the differences in radio properties of the optically and radio-selected SNR samples. We expect that individual interarm SNRs may well have unusual combinations of ambient density, magnetic fields, and shock velocities such that they can produce detectable radio flux densities. This is likely the case for the prominent and unusual interarm SNR 51 (= MF9), which has large radio and X-ray luminosities; the X-ray emission is further evidence of a high ambient density. Inspection of Table 2 shows that five radio-selected interarm SNRs, two of which were also in the optically selected sample of SNRs, had detectable radio emission. The rest of the optically selected SNRs are not detected, indicative of lower average values for the magnetic field and density.

We have shown that particle acceleration can account for the range of observed values of SNR flux densities in NGC 6946 and the nondetection of the interarm SNRs.

6. CONCLUSION

A sample of radio-selected SNRs has been obtained from VLA observations of the nearby spiral galaxy NGC 6946. This sample of equidistant radio-selected SNRs is complete down to a flux density of 60 μJy at 20 cm. The SNRs were identified using techniques described in Lacey et al. (1997).

The positions of the radio-selected SNRs identified in NGC 6946 correlate with the Hα emission associated with the spiral arms and star formation regions. Combining the sample of 35 radio-emitting SNRs with a sample of 27 optically selected SNRs and comparing the positions of the two groups yields the result that optical SNRs with no radio emission lie predominately in the interarm regions, avoiding the spiral arms and concentrations of Hα emission. The radio-emitting SNRs lie predominately on the spiral arms, in or near regions of high star formation. Although these biases can be partially explained in terms of selection effects, we find that an additional explanation is required. K-S tests of the parent distributions of the radio and optically selected SNRs confirm that the radio-selected SNR population is not a random distribution and appears to be correlated with the H II region distribution in NGC 6946. Our results imply, but do not prove, that radio-selected SNRs are cosmic-ray producers and arise from the population of recently formed stars that are found in the high-density regions of the spiral arms.

The difference in radio properties of the arm and interarm populations of SNRs cannot be explained in terms of simple shock compression of the ambient medium. Although such compression does boost the radio emission of the SNRs by a large factor and can account for the *relative* differences between the two populations, it is not possible to account for the *absolute* properties, such as minimum nonthermal energy, in this way.

It is found that Bell's analytical formulation of the DSA mechanism is sufficient to allow for an estimate of the effect of particle acceleration. A comparison of the environmental differences of the arm and interarm regions with their dependencies within the DSA formulation shows that the range of SNR properties can be explained by environmental differences so long as particle acceleration is taking place. It is therefore concluded that because of the richer environments of the arm regions, it is the Type II/Ib/Ic SNRs that are dominant in the production of cosmic rays in NGC 6946.

The authors wish to thank Miller Goss for several useful discussions. C. K. L acknowledges the support of the NRC to support this research.

REFERENCES

Anderson, M. C., & Rudnick, L. 1996, ApJ, 456, 234
Anderson, M. C., Rudnick, L., Leppik, P., Perley, R., & Braun, R. 1991, ApJ, 373, 146
Ball, R., Sargent, A. I., Scoville, N. Z., Lo, K. Y., & Scott, S. L. 1985, ApJ, 298, L21
Bell, A. R. 1978a, MNRAS, 182, 147
———. 1978b, MNRAS, 182, 443
Blair, W. P., & Fesen, R. A. 1994, ApJ, 424, L103
Blair, W. P., Fesen, R. A., & Schlegel, E. M. 2001, AJ, 121, 1497
Chu, Y. -H., & Kennicutt, R. C., Jr. 1988, AJ, 96, 1874
de Vaucouleurs, G. 1979, ApJ, 227, 729
Duffy, P., Lewis, B., & Kirk, J. G. 1995, ApJ, 447, 364
Duric, N., Gordon, S. M., Goss, W. M., Viallefond, F., & Lacey, C. 1995, ApJ, 445, 173
Ehle, M. & Beck, R. 1993, A&A, 273, 45
Ferguson, A. M. N., Wyse, R. F. G., Gallagher, J. S., & Hunter, D. A. 1998, ApJ, 506, L19
Ginzburg, V. L., & Syrovatskii, S. I. 1965, ARA&A, 3, 297
Gordon, S. M. 1993, Ph.D. thesis, Univ. New Mexico
Gordon, S. M., Duric, N., Kirshner, R. P., Goss, W. M., & Viallefond, F. 1999, ApJS, 120, 247
Gordon, S. M., Kirshner, R. P., Long, K. S., Blair, W. P., Duric, N., & Smith, R. C. 1998, ApJS, 117, 89
Lacey, C. K., & Duric, N. 1997, in Proc. 25th Int. Cosmic-Ray Conf. (Durban), 4, 457
Lacey, C., Duric, N., & Goss, W. M. 1997, ApJS, 109, 417
Matonick, D. M., & Fesen, R. 1997, ApJS, 112, 49
Moffett, D. A., & Reynolds, S. P. 1994, ApJ, 437, 705
Pacholczyk, A. G. 1970, Radio Astrophysics: Nonthermal Processes in Galactic and Extragalactic Sources (San Francisco: Freeman)
Reynolds, S. P. 1988, in Galactic and Extragalactic Radio Astronomy ed. G. L. Verschuur & K. I. Kellermann (2d ed.; New York: Springer), 439
Rogstad, D. H., & Shostak, G. S. 1973, A&A, 22, 111
Schlegel, E. M. 1994, ApJ, 424, L99
Tammann, G. A., Löffler, W., & Schröder, A. 1994, ApJS, 92, 487
Taylor, J. H., & Cordes, J. M. 1993, ApJ, 411, 674
van Dyk, S. D., Sramek, R. A., Weiler, K. W., Hyman, S. D., & Virden, R. E. 1994, ApJ, 425, L77
White, R. L., & Becker, R. H. 1992, ApJS, 79, 331